CHARACTERISTICS OF TRANSVERSE OSCILLATIONS IN A CORONAL LOOP ARCADE

E. VERWICHTE[1], V.M. NAKARIAKOV[1], L. OFMAN[2] and E.E. DELUCA[3]
[1]*Department of Physics, University of Warwick, Coventry CV4 7AL, U.K.*
[2]*Catholic University of America/NASA Goddard Space Flight Center, Code 682, Greenbelt, MD 20771 U.S.A.*
[3]*Harvard-Smithsonian Center for Astrophysics, 60 Garden Street, Cambridge, MA 02138, U.S.A.*

(Received 8 March 2004; accepted 15 June 2004)

Abstract. TRACE observations from 15 April 2001 of transverse oscillations in coronal loops of a post-flare loop arcade are investigated. They are considered to be standing fast kink oscillations. Oscillation signatures such as displacement amplitude, period, phase and damping time are deduced from 9 loops as a function of distance along the loop length. Multiple oscillation modes are found with different amplitude profile along the loop length, suggesting the presence of a second harmonic. The damping times are consistent with the hypothesis of phase mixing and resonant absorption, although there is a clear bias towards longer damping times compared with previous studies. The coronal magnetic field strength and coronal shear viscosity in the loop arcade are derived.

1. Introduction

In the last decade the advent of the fleet of space-borne solar observatories such as *Yohkoh*, Solar and Heliospheric Observatory (SOHO) and the Transition Region And Coronal Explorer (TRACE) has turned continuous monitoring of the activity in the solar atmosphere into a reality. The resolutions of the onboard instruments have proven to be sufficient to detect simultaneously clear temporal and spatial signatures of magnetohydrodynamic waves in various coronal structures: propagating slow magnetoacoustic waves in polar plumes (Deforest and Gurman, 1998) and in coronal loops (Berghmans and Clette, 1999), standing slow magnetoacoustic waves in coronal loops (Kliem *et al.*, 2002), global fast magnetoacoustic waves best known as EIT waves (Thompson *et al.*, 1998), and fast magnetoacoustic kink oscillations in coronal loops (Aschwanden *et al.*, 1999; Nakariakov *et al.*, 1999).

Aschwanden *et al.* (1999), Nakariakov *et al.* (1999), Schrijver and Brown (2000), Schrijver, Aschwanden and Title (2002) and Aschwanden *et al.* (2002) analysed EUV TRACE observations that show transverse oscillatory displacements of coro-
nal loops after the occurence of a violent event such as a flare in its vicinity. Aschwanden *et al.* (1999) and Nakariakov *et al.* (1999) have interpreted these oscillations as standing fast magnetoacoustic kink waves, triggered by a passing disturbance that originated from the flare site.

Solar Physics **223:** 77–94, 2004.

The comparison between such wave observations and MHD wave theory allows for the determination of coronal physical parameters of the medium that supports the wave from the wave signatures. This approach is known as MHD coronal seismology (*e.g.* Uchida, 1970; Roberts, Edwin and Benz, 1984; Nakariakov *et al.*, 1999). Especially parameters whose values are not well-established or not open to direct measurements are of interest (e.g., coronal magnetic field strength and dissipation coefficients). Using the dispersion relation of fast kink waves (Edwin and Roberts, 1983), Nakariakov and Ofman (2001) determined the coronal loop magnetic field strength to be in the range 4–30 G.

Nakariakov *et al.* (1999) pointed out that the oscillations experience a quick decay, with a typical e-folding damping time of 870 s. Aschwanden *et al.* (2002) derived from a set of ten loop oscillations an average damping time of 580 ± 385 s. However, it is often difficult to measure the decay time because of the low signal-to-noise ratio.

The damping times of these oscillations are too quick to be explained by the theoretical values of coronal viscosity or resistivity. Therefore, various hypotheses have been put forward to explain the oscillation damping. Nakariakov *et al.* (1999) proposed that the shear viscosity or resistivity is anomalously high, by nine orders of magnitude in comparison with values from Braginskii (1965) and actually of the same order as the bulk viscosity coefficient. Schrijver and Brown (2000) proposed that the transverse oscillation is caused by the response of the location of the photospheric loop footpoints to near-surface solar flares. In their hypothesis the damping rate is fully determined by photospheric conditions. The fact that most observed transverse loop oscillations have a preference to oscillate in a direction parallel to the solar surface as compared to perpendicular cannot be explained by this hypothesis and instead favours a hypothesis where the oscillation is excited by a coronal disturbance from the side. Roberts (2000) compared several possible damping mechanisms. He eliminates optically thin radiation, thermal conduction, wave leakage from curvature and loop footpoints as realistic explanations (see also Cally, 2003). However, De Pontieu, Martens and Hudson (2001) argued by considering more advanced atmospheric models that chromospheric wave leakage may account for the damping after all. But Ofman (2002), using a 1.5D MHD simulation, showed that the oscillation damping due to chromospheric wave leakage exceeds in most cases the observed damping times by a factor five. Roberts (2000) furthermore proposed that the damping rate may be enhanced by the presence of small-scale, transverse inhomogeneities through a mechanism such as resonant absorption. He illustrated this idea with the mechanism of Alfvén wave phase-mixing. Ruderman and Roberts (2002) considered resonant absorption of the global oscillation in which the wave energy is transferred to local, torsional oscillations. Notably, in this model the wave decay does not depend on dissipation.

Ofman and Aschwanden (2002) used the gathered collection of observations of Aschwanden *et al.* (2002) to test the hypothesis of phase mixing (Roberts, 2000) and ideal kink wave damping (Ruderman and Roberts, 2002). They concluded from

scaling relations involving the oscillation parameters and loop structure, that the observations match best the hypothesis of phase mixing, although the hypothesis of resonant absorption could not be ruled out. In the phase mixing model, the observationally deduced shear viscosity coefficient is at least five orders of magnitudes larger than theory predicts (Braginskii, 1965), in agreement with the earlier findings of Nakariakov *et al.* (1999). Ofman and Aschwanden (2002) argued that the viscosity is enhanced by small-scale turbulence or kinetic processes.

Goossens, Andries, and Aschwanden (2002) argued that the quick decay of the kink oscillations could still be explained in terms of resonant absorption, provided the ratio of the inhomogeneity length scale to the radius of the loop is allowed to vary from loop to loop. However, the exact reproduction of the observationally determined decay times would require the loop cross-section to be sufficiently smooth, which is not consistent with the assumption of a thin boundary layer used to obtain this analytical result. Aschwanden *et al.* (2003) develop that study further, attempting to test observationally the analytical expressions for the period and damping time due to resonant absorption, derived for loop models with thin nonuniform boundaries. Thickness of the nonuniform layer in oscillating loops is estimated for 11 events analysed by Ofman and Aschwanden (2002). It is found that the density ratio predicted by the damping time, is a factor of $\sim 1.2-3.5$ higher than the observationally estimated density ratio. This discrepancy is suggested to be connected with the narrowness of TRACE bandpasses.

De Moortel, Hood and Ireland (2002) re-analysed the event discussed by Aschwanden *et al.* (1999) and Nakariakov *et al.* (1999) and two additional events, checking whether the exponential decay law gives the best fit of the observational data. It is suggested that the best approximation may be given by the $\exp(-t^n)$-law with a constant parameter n.

Certainly, the results obtained with the use of only 11 or less oscillating loops cannot be considered as statistically significant, especially taking into account the low signal-to-noise ratio. The further development of this study requires a serious improvement of the statistics.

The contribution of this paper to the understanding of the transverse oscillations, is a detailed observational study of the oscillatory behaviour of an ensemble of several loops forming an arcade. The event analysed contains about 9 distinct oscillating loops, allowing for the determination of the oscillation parameters such as oscillation periods, phases, amplitudes and damping times with reasonable accuracy. The observational data set used in this paper has originally briefly been analysed by Reeves *et al.* (2001). Schrijver, Aschwanden and Title (2002) and Aschwanden *et al.* (2002) later reanalysed this data set, but the result has not been considered in the context of the scaling laws discussed above.

There have been just a few theoretical studies of the interaction of MHD waves with coronal arcades and the main attention was paid to the evolution of vertically propagating waves and to normal modes. In particular, propagation of impulsively generated waves in coronal arcades was simulated numerically by Oliver, Mur-

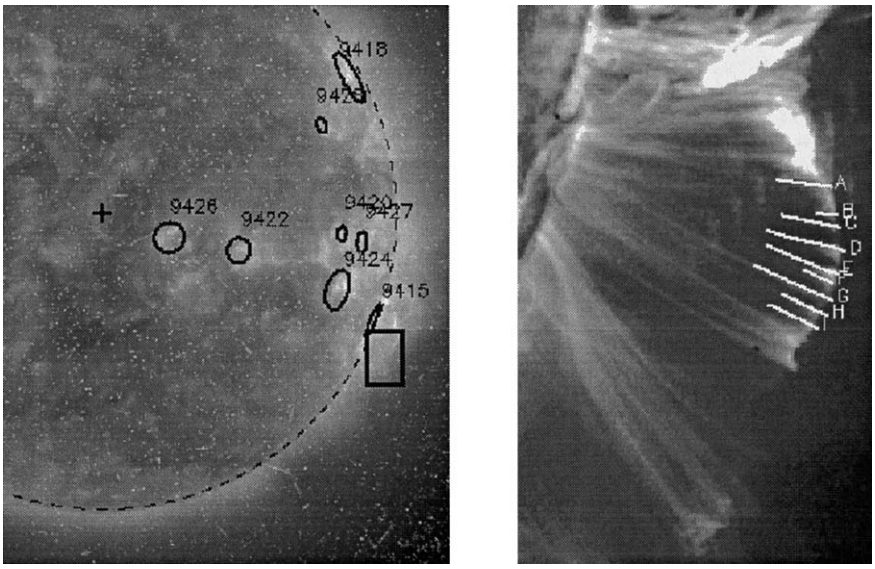

Figure 1. Left: Subfield of a 195 Å EIT/SOHO full-disk image on 15 April 2001 at 20:24 UT with NOAA active regions and field of view of the TRACE subfield. *Right*: Subfield of TRACE observation on the same day at 22:11 UT with paths used in the analysis.

awski, and Ballester (1998). Modes of oscillation of potential and nonpotential magnetic arcades have been studied by Terradas, Oliver, and Ballester (1999). Developing this study, Arregui, Oliver, and Ballester (2001) modelled normal modes of arcades with a shear, considering coupling of compressible and incompressible modes.

The paper is structured as follows. In Section 2 the details and context of the TRACE observation are given. In Section 3 the procedure for the determination of the oscillation signatures is set out. Furthermore the determined wave parameters are discussed. In the final section these results are compared with previous studies. Also the coronal magnetic field strength and viscosity coefficient are determined from the wave parameters.

2. Description of the Observation

The present study focuses on the 171 Å wavelength observations from the TRACE instrument (Handy *et al.*, 1999) on the 15th of April 2001 between 22:00:43 and 22:27:50 UT. The temporal cadence of the sequence in the first 20 min is equal to 26 s, but in the last 10 min increases to one minute. The spatial resolution of the TRACE instrument is one arcsecond.

The instrument was pointing to the active region NOAA 9415, then on the southwestern limb. This active region was at the time active and produced at 13:48 UT a GOES X-ray class X14.4 flare and following smaller flares. The flare

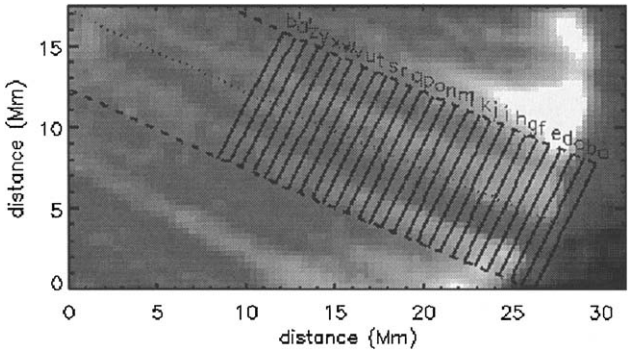

Figure 2. Path G with location of image sets $I_{G,x}$ overlaid on data at 22:11 UT.

activity resulted in a postflare loop arcade that was first seen by TRACE at 14:40 UT. Because the active region is close to the solar limb and the arcade axis lies quasi-meridionally, the spacecraft looks along the plane of the arcade loops. The two loop legs are in the same line of sight. This arcade is disturbed by a prominence eruption nearby to the north, which presumably is the cause of the transverse oscillations in the arcade loops. The transverse loop oscillations appear as a back and forth motion of the loop plane. At first glance, the oscillation period is of the order of five minutes and 2–2.5 oscillation cycles can be clearly distinguished. Furthermore, the oscillation amplitude decays with time. However, it is difficult to identify individual oscillating loops due to the superposition of shifting loops and/or the two legs of the same loop. For example the loop in path G seems at times double, where the two parts oscillate with the same amplitude, period and phase. This suggests that the two parts are the two legs of the same loop that are seen almost along the same line of sight.

3. Analysis of Oscillation Signatures

Nine paths are constructed using a polynomial, fourth-order fit of each coordinate of a series of points that are selected by eye to follow a loop in one particular image (at 22:11 UT). As can be seen in Figure 1, the paths are essentially straight lines. From each path a uniform grid is built that is fixed in time and has a width of 25 pixels, which is sufficiently wide to include neighbouring loops and to capture the transverse motions of the loop. On each grid point the intensity $I_p(t, x, y)$ is interpolated, where x and y are the longitudinal and transversal projected coordinates in the plane of the sky respectively. The longitudinal coordinate x is measured from the path top, near the loop top, downwards.

Table I shows the spatial path and loop details for each path. The loop length, L, is calculated by assuming that the height of the loop top above the solar limb, H, is the radius of a circular loop. The analysed x-interval is the path segment,

TABLE I
Path parameters.

Path	Δx (Mm)	H (Mm)	L (Mm)	$\Delta s/L$
A	9	65	203	0.17
B	5	68	214	0.12
C	12	70	218	0.19
D	18	73	228	0.23
E	10	74	233	0.17
F	7	74	233	0.14
G	15	76	237	0.20
H	7	75	235	0.14
I	12	75	236	0.18

Δx is the analysed x-interval, H is the loop height defined as the projected distance between the loop top and the solar limb and L is the length of a circular loop with radius H. The analysed loop fraction, $\Delta s/L$, is the fraction of the circular loop that is covered by Δx, and is calculated as arc cos $((H - \Delta x)/H)/\pi$. If the superposition of the loop legs is taken into account, this fraction needs to be doubled.

measured from the loop top, that has been included in the further analysis. At greater distances down the loop, the loop intensity signal becomes uncertain as it is superimposed on lower lying loops. The analysed loop fraction is the corresponding fraction of the length of a circular loop that the x-interval represents. Since the two loop legs are in the same line of sight, the observed loop fraction is in reality twice as long.

For fixed positions x, at two pixel intervals (corresponding to a distance of 0.7 Mm), the sets of segment images $I_{p,x}(t, y)$ are examined. Figure 2 shows as an example path G with the location of the segments $I_{G,x}(t, y)$ overlaid. These segment images show the transverse position of the loop width as a function of time and are therefore ideal for detecting transverse loop oscillations.

The position of the centre of the loop width is captured in segment images $I_{p,x}(t, y)$ interactively by selecting by eye sets of coordinate pairs (t_i, y_i) that follow the loop profile. Figure 3 shows as an illustration four segment images at different positions along the loops D and G. The measurement error takes into account the interactive selection (set at spatial resolution) and the temporal cadence. An automatic method (e.g., finding the spatial maximum at fixed times) would be preferable if it was not for the frequent loop superpositions that lead the method astray. For example, in path C the examined loop overlaps in the last ten minutes with another loop. The resulting superposition gives the false impression that the loop oscillation amplitude is growing. The human eye is in such cases superior in

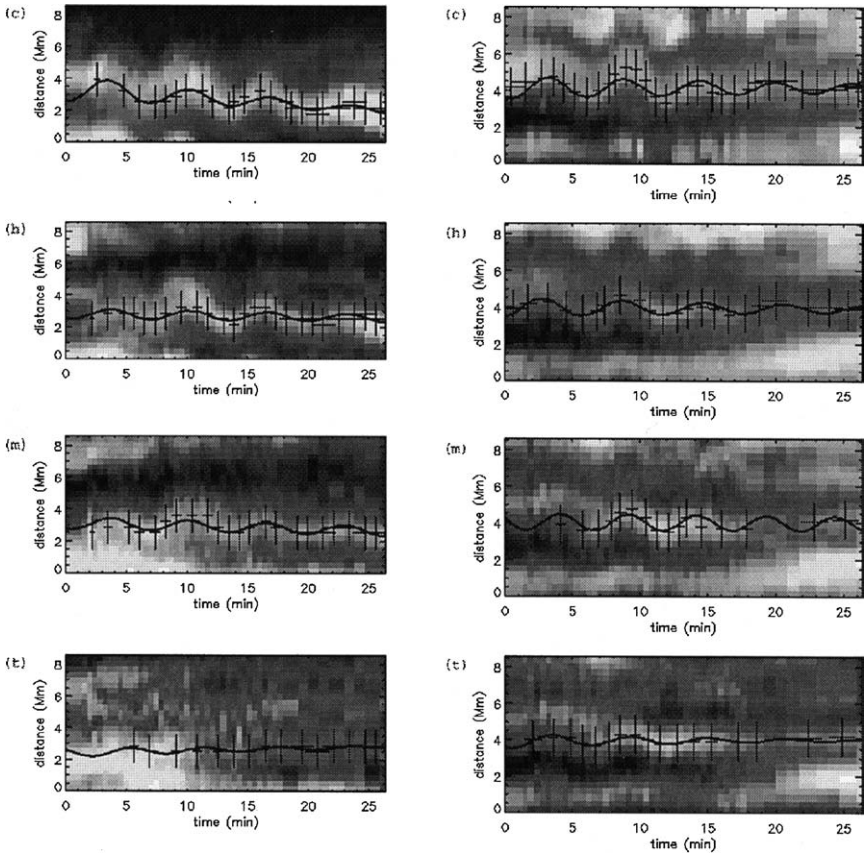

Figure 3. Left: Set of four images $I_{D,x}(y, t)$ of the segments c, h, m, and t, corresponding to $x = 0.7$, 3.6, 6.4, and 10.0 Mm from the loop top, respectively, along the loop in path D. The displacement coordinates are shown as crosses. The *solid curve* is a fitted function of the form (1) with $n = 1$. *Right*: Same as before, but for path G. The segments c, h, m, and t correspond to $x = -0.1$, 3.5, 7.1, and 10.6 Mm from the loop top, respectively.

disentangling the scene, but this subjectivity may also cause systematic errors. For a clear example, without superposition, the interactive approach has been compared to an automated method based on finding for each time t the position of the centre of the loop profile by fitting a superposition of a linear and Gaussian profile to the intensity. In this case, the two methods produced similar results.

Besides the loop oscillation, the loop position also shifts slowly in time. This is estimated with a linear fit $y_{lin,i}\,(t_i)$. The position $\xi_i = y_i - y_{lin,i}$ is considered as the displacement of the loop centre from the equilibrium position at fixed position x along the loop. Two approaches for examining the displacement coordinates (t_i, ξ_i) have been chosen. Firstly, a wavelet analysis is performed, using the software provided by Torrence and Compo (1998). The coordinates are resampled to a regular time step of 26 seconds and used as input for a 1d wavelet transform

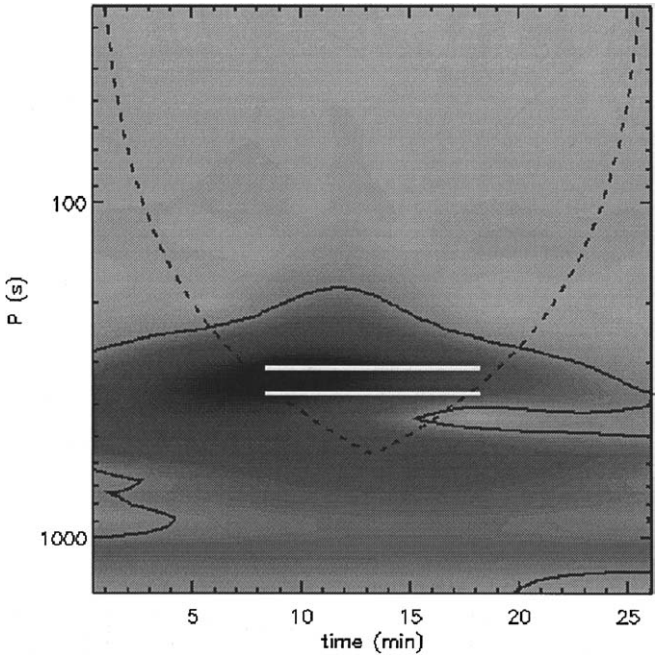

Figure 4. Magnitude of the one-dimensional wavelet transform with the Morlet wavelet of the displacement coordinates (t_i, ξ_i) from image $I_{G,c}(y, t)$ of path G, as a function of time and period. The segment c corresponds to a distance $x = -0.1$ Mm from the looptop. The *solid line* is the 95% confidence level. The *black, dashed line* shows the cone of influence of the edges of the time series. The *white lines* show the location of the detected wave signal from which the wave parameters $A = 750$ km, $P = 338$ s, and $\phi = 140°$ are deduced.

with the Morlet mother wavelet. The Morlet wavelet is apt for detecting quasi-periodic signals. The resulting wavelet transform is a convolution that is a function of time and period. Statistically significant signals are extracted and the period, amplitude and phase of the quasi-periodic oscillation determined. Figure 4 shows an example of a wavelet transform. The dashed line denotes the cone of influence of the edges of the time series. Only results outside of the cone are considered. The full black line is a contour of the 95% confidence level. The two white lines bracket as a function of time the position of a maximum in period of the wavelet power, which is statistically significant and which lies outside of the cone of influence of the edges. It is also possible to determine information about the damping of the signal (De Moortel and Hood, 2000; De Moortel, Hood, and Ireland, 2002). The temporal evolution of the amplitude extracted from the wavelet transform is in essence a convolution of the real amplitude profile with a gaussian with a width equal to the oscillation period. Because the damping time is not much longer than the oscillation period, the amplitude evolution is blurred. Therefore the damping time is not determined from the wavelet analysis.

Secondly, the displacement coordinates (t_i, ξ_i) are fitted, using non-linear least-squares, with a single, damped oscillation mode of the form

$$\xi_n(t) = Ae^{-\gamma_n t^n} \cos(\omega t + \phi), \tag{1}$$

where $P = 2\pi/\omega$ and $\tau_n = \gamma^{-1/n}$ are the period and e-folding damping time, respectively. The values for n of 1, 2, and 3 have been applied. The parameters determined from the wavelet transform are used as first estimates in the curve fitting. The solid curves in Figure 3 are curves of the form (1) for $n = 1$.

Overall the results from the wavelet analysis and the curve fitting are consistent. It is clear though, that the wavelet transform has the advantage over the curve fitting method in that it can detect multiple periods and period modulations. When this occurs the parameters of the curve fitting may be a mix from multiple contributions, especially when the amplitudes are comparable. The results from this method are then unreliable.

For each segment in the x-direction along the examined loop of each path, the oscillation parameters, i.e., P, A, ϕ, and τ_n, are determined. For the former three parameters a weighted average is calculated from the measurements for different n. Furthermore a weighted average across x is taken. If a clear trend as a function of x is observed or is expected, then alternatively a weighted linear least-squares fit is calculated. The results are presented in Tables II and III.

For the loops in paths A, B, and F it has not been possible to track their position reliably the whole time due to superpositions with neighbouring, brighter loops. Also, for the same reason, the displacement measurements are noisier than for other loops. The determined parameters from the curve fitting are therefore less reliable. Especially for the damping time, which is more sensitive to noise than the period as it varies slower than the oscillation with time, the error is large. Furthermore the value of the damping time varies too much from segment to segment along each of these loops. Therefore the damping times for these loops have not been included in Table II. The wavelet analysis could not pick up any significant peaks in period for loops B and F.

For periods and damping times no x-dependency is seen. In other words, different segments of the analysed loop are observed to oscillate in phase and each loop segment damps at the same rate. The oscillation periods are in the range 200–450 s, which is typical for transverse loop oscillations (Aschwanden *et al.*, 2002). Furthermore the periods obtained from the wavelet analysis and from the curve fitting method are mutually consistent.

All the measured loop oscillations are damped, with damping times in the range of 800–1800 s. The range of oscillation periods and damping times are consistent with the results of Reeves *et al.* (2001). A clear distinction between the different damping profiles used in the curve fitting ($n = 1$, 2, or 3) cannot be made.

If the observed oscillation is a standing wave, then it is expected that the displacement amplitude should vary with distance while the phase remains constant.

For a circular, homogeneous loop with its loop plane in the line of sight, the amplitude of the fundamental mode is expected to be of the form

$$A(x) = A(x_{\text{top}}) - (A(x_{\text{top}})/H)x, \tag{2}$$

where H is the loop height. Using the previous formula and considering that $A\left(x_{\text{top}}\right)$ and H lie in the ranges 100–600 km and 65–76 Mm respectively, the amplitude in the observed loops is expected to decrease as a function of x by a value of the order of -5 km Mm^{-1}. On the other hand if the oscillation is a second harmonic standing mode, the displacement has a node at the loop top. The spatial dependency of the amplitude is then of the form

$$A(x) = A_{\text{max}} \sin(2 \arccos(\left(H - x + x_{\text{top}}\right)/H)). \tag{3}$$

Near the loop top the amplitude is therefore expected to increase as a function of x.

In most cases the sign of the slope of the amplitude is negative, implying that the amplitude decreases with distance from the loop top. The value of the slope is though often of low statistical confidence. Furthermore in almost all cases the phase does not show any trends as a function of x. These results are in agreement with a fundamental fast kink mode oscillation. The loops in paths C and D are different from the other loops as they show multiple modes of oscillation. These two cases will be discussed in more detail below.

The first 12 Mm from the loop top of the loop in path C are examined. For most positions along the path an oscillation with a period of 250 s is found. But at several positions, especially away from the loop top, the wavelet analysis reveals two significant periods. Besides the 250-s-period oscillation, there is also an oscillation mode with a period around 450 s. The 450-s period falls within 1 standard deviation of the double of the 250-s period, i.e., $|P_{450} - 2P_{250}|/\sqrt{2}\sigma_{250} \approx 1$, where σ_{250} is the error (standard deviation) of the 240-s-period measurement. The curve fitting method picks up the 250-s-period oscillation mode, except at two positions (at x equal to 5.5 and 11 Mm) where the other mode is found.

In the presence of two oscillation modes, the fitting of the measurements with a curve consisting of a single oscillating frequency may yield inaccurate results, especially if the oscillation amplitudes are similar. Therefore in this case the period, amplitude and phase from the wavelet analysis are preferred. The displacement amplitude of the 450-s-period oscillation decreases with distance from the loop top at a rate of 25 ± 14 km Mm^{-1}. This is actually confirmed by the curve fitting method. On the other hand the amplitude of the 250-s-period oscillation does not change statistically over the analysed distance. The damping times are taken from those measurements where the curve fitting method clearly picks up one of the two oscillation modes. This is the least succesful for the case $n = 1$. For the 250-s and 450-s-period oscillation modes typical damping times of around 900 s and 1450 s are found respectively. This corresponds to a damping by a factor e^{-1} in about 3.2 and 3.6 oscillation periods, respectively.

TABLE II

Periodicity and damping of transverse loop oscillations

Path	Wavelet P (s)	Fit P (s)	τ_1 (s)	τ_2 (s)	τ_3 (s)
A	301 ± 50	326 ± 107	–	–	–
B	–	393 ± 77	–	–	–
C	247 ± 33	315 ± 144	$(980)^{(a)}$	920 ± 290	860 ± 300
	448 ± 18	(405 ± 35)	–	(1550 ± 640)	(1400 ± 320)
D	242 ± 31	–	–	–	–
	396 ± 20	392 ± 31	1180 ± 1050	1780 ± 560	1840 ± 580
E	379 ± 54	382 ± 12	1320 ± 570	1350 ± 480	1180 ± 340
F	–	243 ± 103	–	–	–
G	346 ± 78	358 ± 30	1030 ± 680	1060 ± 420	920 ± 260
H	317 ± 80	326 ± 45	960 ± 420	1010 ± 380	930 ± 310
I	325 ± 107	357 ± 89	(960 ± 760)	1400 ± 580	1360 ± 650

Values between brackets are uncertain measurements.
[(a)] Based upon one measurement.

TABLE III

Displacement amplitude and phase of transverse loop oscillations

Path	$A(x)$ (km)	$\phi(x)$ (deg)
A	$453 \pm 140 - (34 \pm 27)x$	231 ± 38
B	$(156 \pm 188 + (30 \pm 52)x)$	184 ± 94
C	$342 \pm 66 + (1 \pm 12)x$(a)	$102 \pm 112^{(a)}$
	$430 \pm 109 - (25 \pm 14)x^{(a)}$	$7 \pm 188^{(a)}$
D	$(135 \pm 66 + (14 \pm 7)x)^{(a)}$	–
	$487 \pm 77 - (13 \pm 9)x$	$183 \pm 9 - (6.6 \pm 1.7)x^{(b)}$
E	$424 \pm 69 - (10 \pm 12)x^{(c)}$	191 ± 18
F	–	176 ± 143
G	$557 \pm 68 - (12 \pm 14)x$	171 ± 65
H	$(218 \pm 50 - (8 \pm 9)x)^{(a)}$	172 ± 92
I	$238 \pm 86 - (6 \pm 12)x$	143 ± 76

Values between brackets are uncertain measurements.
[(a)] Based upon estimates from wavelet analysis.
[(b)] Linear trend in phase observed for $x < 10$ Mm.
[(c)] Based upon measurements for $x < 7$ Mm.

The loop central in path D is analysed along a distance of 18 Mm measured from the loop top. The left hand side of Figure 3 shows the displacement as a function of time at four segments along the loop. The main results of the measured periods and amplitudes as a function of distance are shown in Figure 5. The curve-fitting method confidently finds, as shown in plot (b) of Figure 5, for distances within 15 Mm from the loop top an oscillation mode with a period of 400 s. This period is also found by the wavelet analysis. At distances beyond 15 Mm the measured periods have a growing spread. This is probably because of a growing error in the selection of the displacement coordinates at larger distances where the loop's visibility decreases, although it may also be affected by the presence of a second oscillation mode. Namely, from distances of 5 Mm onwards from the loop top the wavelet analysis finds a second significant oscillation mode with a period of about 240 s. Plot (a) of Figure 5 shows an example of the wavelet transform at a distance of $x = 11$ Mm from the loop top. Two periods are detected. The value of the 400-s-period oscillation is within two standard deviations from double the 240 s period oscillation, i.e., $|P_{400} - 2P_{240}|/\sqrt{2}\sigma_{240} \approx 2$, where σ_{240} is the error (standard deviation) of the 240-s-period measurement.

The displacement amplitude of the 400-s-period oscillation mode clearly diminishes with distance with a linear slope of 13 ± 6 km Mm^{-1} (see plot (c) in Figure 5). On the other hand, using the wavelet measurements of the 240-s oscillation for $x < 8$ Mm, the amplitude of this mode shows an increase, with a linear slope of 17 ± 7 km Mm^{-1} (see plot (d) of Figure 5). The solid lines in plot (d) of Figure 5 are the displacement curves of a second harmonic with the appropriate loop height, for several values of the amplitude $A_{\max}$. A value of $A_{\max} = 350$ km seems the most realistic. Though, in order to obtain this result, two measurements at $x > 8$ Mm have been neglected that did not follow this trend. This is justified by the previously mentioned argument that with distance along the loop the errors in the detection of the loop displacement are expected to grow.

The phase of the 400-s-period oscillation mode is interesting. It decreases linearly for distances within 10 Mm of the loop top. It is observed that the phase decreases by -6.6 deg Mm^{-1}. This could be interpreted as a travelling wave solution with a wavelength of 55 Mm and which propagates down the loop.

4. Discussion

For the above observations of paths C and D the following hypothesis is proposed. The long-period oscillation is the fundamental mode, with a maximum amplitude at the loop top. The short period oscillation is its second harmonic. It has a node at the loop top and assuming the loop is circular and homogeneous, the position of the maximum amplitude, $x_{\max}$, by taking $A(x_{\max}) = A_{\max}$ in Equation (3), is equal to $x_{\max} - x_{\text{top}} = \left(2 - \sqrt{2}\right) H/2$. For both loops C and D the value of H is

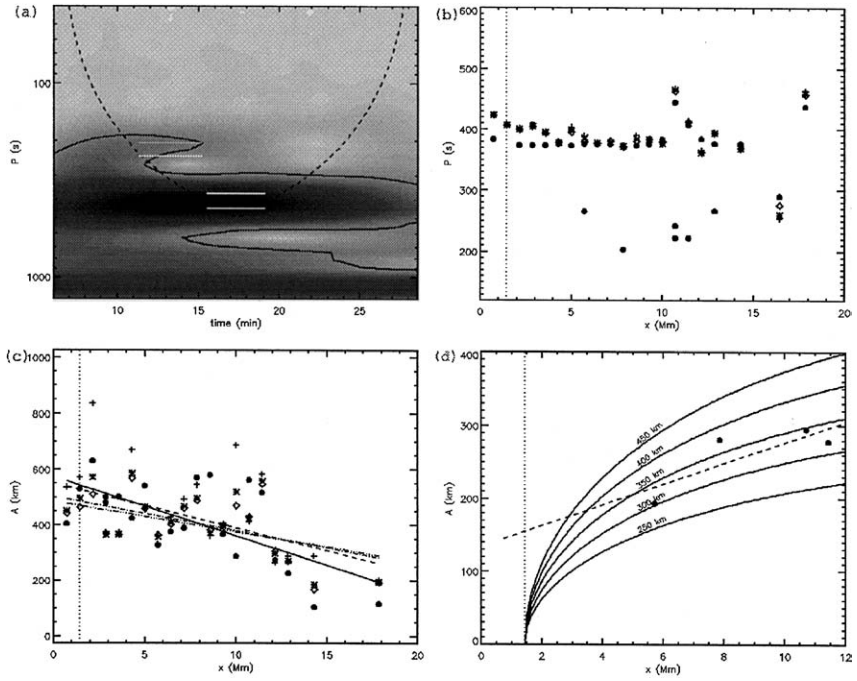

Figure 5. Overview of the period and amplitude of the loop oscillations in path D. (a) magnitude of the wavelet transform of the displacement coordinates of $I_{D,x}$ at $x = 11$ Mm from the loop top. The *white lines* bracket the two detected periodic signatures at 240 and 400 s, respectively. (b) measured oscillation periods as a function of distance x. The *solid circles* are the periods found with the wavelet analysis. The *crosses, stars*, and *diamonds* are the periods derived by the curve fitting method with $n = 1$, 2, and 3, respectively. (c) Displacement amplitude A for the 400 s oscillation as a function of distance x. The *crosses, stars*, and *diamonds* are the amplitudes derived by the curve fitting with $n = 1$, 2, and 3, respectively. The circles are the amplitudes found with the wavelet analysis. Each dataset is fitted by a straight line (*solid*: wavelet fit, *dashed*: $n = 1$, *dot-dashed*: $n = 2$, *triple dot-dashed*: $n = 3$). (d): Displacement amplitude A for the 240 s oscillation. Only wavelet measurements are available and are shown as circles. The *dashed line* is a linear fit. The *solid curves* represent the profile of a second harmonic standing mode for several amplitude values. The *dotted line* in plots (b), (c), and (d) shows the position x_{top} of the loop top.

in the range 70–73 Mm. Therefore $x_{\max} = 20.5$–21.4 Mm, roughly 20 Mm from the loop top.

The phase shift observed in the loop in path D, though, may indicate transient behaviour.

From the measured oscillation parameters, physical quantities can be derived. The transverse oscillation is considered to be a standing fast magnetoacoustic kink oscillation (Aschwanden *et al.*, 1999; Nakariakov and Ofman, 2001). In the limit of the loop width much smaller than the oscillation wavelength, the phase speed of such type of waves, is approximately equal to the kink speed, C_k, i.e.,

TABLE IV
Derived physical parameters

Path	C_k (km s^{-1})	V_A (km s^{-1})	B (G)	ν (m^2 s^{-1})	R
A	1250 ± 410	$880 - 1000$	$13 - 36$	–	–
B	1090 ± 210	$770 - 880$	$11 - 31$	–	–
C	880 ± 120[(a)]	$620 - 700$	$9 - 25$	$0.9 - 1.4 \times 10^8$[(a)]	$1.0 - 1.7 \times 10^6$
	970 ± 40	$690 - 790$	$10 - 28$	$0.6 - 1.0 \times 10^8$	$1.4 - 2.9 \times 10^6$
D	940 ± 120[(a)]	$670 - 760$	$10 - 27$	–	–
	1160 ± 90	$820 - 940$	$12 - 33$	$0.3 - 0.4 \times 10^8$	$4.4 - 7.6 \times 10^6$
E	1220 ± 40	$860 - 980$	$13 - 35$	$0.8 - 1.5 \times 10^8$	$1.4 - 3.0 \times 10^6$
F	1920 ± 810	$1360 - 1550$	$20 - 55$	–	–
G	1320 ± 110	$940 - 1070$	$14 - 38$	$1.4 - 2.8 \times 10^8$	$0.8 - 1.8 \times 10^6$
H	1440 ± 200	$1020 - 1160$	$15 - 41$	$1.3 - 2.2 \times 10^8$	$1.1 - 2.0 \times 10^6$
I	1320 ± 330	$940 - 1070$	$14 - 38$	$0.6 - 0.9 \times 10^8$	$2.6 - 4.1 \times 10^6$

[(a)]Oscillation is assumed to be a second harmonic.

$$V_{\text{phase}} = \frac{2L}{jP} \approx C_k = \sqrt{\frac{2}{1 + \rho_e/\rho_0}} V_{\text{A}}, \tag{4}$$

where j is the wave mode. ρ_0/ρ_e is ratio of the mass density of the loop and its external surroundings. It is assumed (see Nakariakov and Ofman, 2001 for discussion) that this ratio realistically lies in the range 0–0.3. In general the fundamental mode, i.e., $j = 1$, is taken, except for the two 240-s oscillations in paths C and D for which the second harmonic, i.e., $j = 2$, is taken. V_{A} is the Alfvén speed. Thus, by utilizing the determined oscillation period P and wavelength $2L/j$, the local Alfvén speed is determined from Equation (4). It lies in the range 700–1300 km s^{-1}. The obtained kink and Alfvén speeds are listed in Table IV. Note that the uncertainty of the value of L has not been taken into account in this calculation. The uncertainty in the kink speed is therefore solely due to the uncertainty in the period. Since we expect the relative uncertainty in the loop length to be approximately the same for all loops, the uncertainty in the kink speed is an indicator of the relative quality of the measurements.

From the Alfvén speed, by considering a realistic number density of $(1–6) \times 10^{15}$ m^{-3}, the magnetic field strength in the coronal loop, B, is estimated. The result lies for all the loops in the range of 9–46 G. This is in general agreement with the result from Nakariakov and Ofman (2001).

Ofman and Aschwanden (2002) compared the predictions of the various hypotheses explaining the oscillation damping with the collected database of transverse oscillations of Aschwanden *et al.* (2002). They concluded that of the examined

hypotheses the phase-mixing hypothesis proposed by Roberts (2000) fits the observations best. The damping time in this case is equal to (Roberts, 2000)

$$\tau = \left(\frac{6L^2}{\nu \pi^2 V_{\rm A}'^2 j^2} \right)^{1/3}, \tag{5}$$

where ν is the coronal, kinematic, shear viscosity coefficient. $V_{\rm A}'$ is the spatial gradient of the Alfvén speed in the direction both perpendicular to the loop-axis and the oscillation displacement. As an approximation it is assumed that $V_{\rm A}'$ is equal to $V_{\rm A}/\ell$, where the ratio $\ell/L \ll 1$. Here the constant value of 0.01 is chosen for this ratio. Of course, as Goossens, Andries and Aschwanden (2002) and Aschwanden *et al.* (2003) argued, this ratio may in fact vary from loop to loop. If we assume that the oscillation is damped by the process of phase mixing, then from Equation (5) with $V_{\rm A}' \approx V_A L/0.01$, the shear viscosity coefficient can be derived. We found the kinematic shear viscosity to be in the range $(0.3–2.8) \times 10^8$ m^2 s^{-1}. The corresponding shear Reynolds number, $R = LV_{\rm A}/\nu$, is in the range $(0.8–7.6) \times 10^6$. These values are consistent with those found by previous authors Ofman and Aschwanden (2002). If the loop temperature is assumed to be that of the instrument bandpass, i.e., 1 MK, and the previously mentioned number density is considered, then from Braginskii (1965) the theoretical shear Reynolds number is calculated as

$$R_{th} = \frac{10 L V_{\rm A} \tau_i \omega_{ci}^2 m_i}{3 k_B T_i}, \tag{6}$$

where k_B is the Boltzmann constant and T_i, τ_i, ω_{ci}, and m_i are the temperature, collision time, cyclotron frequency and mass for ions, respectively. For typical coronal conditions, the theoretical shear Reynolds number is of the order of 10^{14}. There is a discrepancy of eight orders of magnitude between the observational and theoretical values of the Reynolds number. On the other hand, the observationally derived Reynolds number is of similar order as the theoretically expected compressive Reynolds number.

By combining Equation (4) with the approximated version of Equation (5) with a constant ratio L/ℓ, Ofman and Aschwanden (2002) deduced that the damping time is related to the oscillation period as $\tau \sim P^{4/3}$. On the other hand, the mechanism of resonant absorption predicts that $\tau \sim P$. The 11 compiled oscillation observations considered by Ofman and Aschwanden (2002) show a dependency of $\tau \sim P^{1.17 \pm 0.35}$. The predictions of both hypothesis fall within one standard deviation from the observational result. By removing two apparently outlying measurements, though, they found a dependency of $\tau \sim P^{1.30 \pm 0.12}$, which clearly favoured the hypothesis of phase mixing. Figure 6 shows as filled circles the damping times of the measured loop oscillations as a function of their period of oscillation. The diamond symbols indicate the compiled oscillation observations considered by Ofman and Aschwanden (2002). The solid line represents a best

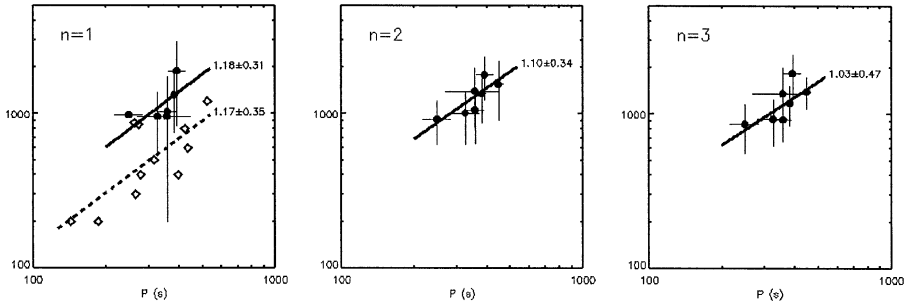

Figure 6. Plot of the measured decay times τ with respect to the oscillation period P as *solid circles* for the cases $n = 1, 2, 3$. The *diamond symbols* show the measurements from (Nakariakov *et al.*, 1999) and (Aschwanden *et al.*, 2002) that were used by Ofman (2002) to deduce the powerlaw relationship $\tau \sim P^{1.17\pm0.35}$, here shown as a *dashed line*. The *solid line* is a best powerlaw fit of the measurements of this loop arcade. The value of the power index of each powerlaw fit is shown. The powerlaw fit for $n = 1$ includes two outlying measurements from (Ofman, 2002). Without these no reasonable fit is possible for $n = 1$.

powerlaw fit. For $n = 1$ a reliable powerlaw fit is not possible from the measurements of this loop arcade because the data points cover only a narrow range of periods. The two measurements that Ofman and Aschwanden (2002) considered to be outliers actually fall into the same range. Although no clear justification can be made beyond this observation, if these two measurements are added to our measurements, a powerlaw relation $\tau \sim P^{1.18\pm0.31}$ is found. The power index is in agreement with the one derived by Ofman and Aschwanden (2002). For $n = 2$ and $n = 3$ the powerlaw relations $\tau \sim P^{1.10\pm0.34}$ and $\tau \sim P^{1.03\pm0.47}$, respectively, are found. They do not differ significantly from the case $n = 1$ and the result of Ofman and Aschwanden (2002). These results also do not allow to distinguish between the two oscillation damping hypothesis. The first thing that is immediately clear from the figure is that the damping times found in this study have a systematic bias towards longer decay times compared with most of those found previously. There are several possible explanations for this bias. Firstly, this study considered an oscillating arcade of post-flare loops. The other cases are all more isolated oscillating active region loops. We may not be comparing the same type of structures. Besides, the structure of post-flare loops may be different from active region loops, the damping times of the loop oscillations may also be influenced by the interactions between the different oscillating loops in the arcade. Secondly, the coronal loop arcade oscillation is driven by a prominence eruption in its vicinity, that excites the arcade at several occasions. In fact at a time between 22:00 and 22:10 UT the prominence is seen to be shifting southwards towards the arcade. This event may have fed fresh impulses to the loop oscillations. If a time of 5–10 min is subtracted from all the damping times from this study, then they fall in the range of the decay times of the earlier studies. The relationship between damping time and period, though, would then be much steeper.

5. Summary

TRACE observations of transverse oscillations of nine loops in a coronal post flare arcade have been examined in order to improve the statistics of measurements of transverse oscillations and to further the development of mechanisms that explain the rapid damping rate. The period, decay times, phase and amplitude have been determined as a function of position along the loop. The periods for all the loops lie within the range of 240–450 s. The phase remains in all but one case constant and the displacement amplitude is in most cases observed to decrease from the loop top. These results are consistent with fundamental standing fast magnetoacoustic kink oscillations. From the phase speed of the oscillation the magnetic field strength has been derived to be in the range 9–46 G, which is consistent with previous measurements.

In two loops two oscillation modes have been observed simultaneously. The long period oscillation is marginally double the short period. Also, the amplitude of the short period oscillation decreases with distance from the loop top. This suggests that the short period oscillation may be the second harmonic kink mode.

The range of damping times is 860–1800 s, which is in the order of 5 to 10 min longer than expected from previous observations of transverse oscillations within the same period range. We suggest this is due to the different nature of post flare loops compared to active region loops and/or the different manner the oscillations are excited here. The observations show a scaling relationship between damping time and period that is consistent with previous measurements. The uncertainty on the scaling law and the lack of preference for a decay profile, i.e., $n = 1$, 2, or 3, do not allow us to distinguish between the mechanisms of resonant absorption and phase mixing put forward to explain the rapid decay. If we assume that the phase mixing mechanism correctly describes the oscillation damping, then the coronal shear kinematic viscosity can be derived. We find values of the shear Reynold number in the range of $(0.8–7.6) \times 10^6$, which differ with the theoretically expected value by eight orders of magnitude.

Acknowledgements

Erwin Verwichte is grateful to PPARC for the financial support. Leon Ofman would like to thank support by NASA Sun-Earth Connection Theory program. The authors would like to thank an anonymous referee for helpful comments.

References

Arregui, I., Oliver, R., and Ballester, J. L.: 2001, *Astron. Astrophys.* **369**, 1122.
Aschwanden, M. J., Fletcher, L., Schrijver, C. J., and Alexander, D.: 1999, *Astrophys. J.* **520**, 880.
Aschwanden, M. J., De Pontieu, B., Schrijver, C. J., and Title, A. M.: 2002, *Solar Phys.* **206**, 99.

Aschwanden, M. J., Nightingale, R. W., Andries, J., Goossens, M., and Van Doorsselaere, T.: 2003, *Astrophys. J.* **598**, 1375.
Berghmans, D. and Clette, F.: 1999, *Solar Phys.* **186**, 207.
Braginskii, S. I.: 1965, *Rev. Plasma Phys.* **1**, 205.
Cally, P. S.: 2003, *Solar Phys.* **217**, 95.
Curdt, W., Wang, T. J., Innes, D. E., Solanki, S. K., Dammasch, I. E., Kliem, B., and Ofman, W.: 2002, *ESA SP-506*, 581.
Deforest, C. E. and Gurman, J. B.: 1998, *Astrophys. J. Lett.* **501**, L217.
De Moortel, I. and Hood, A. W.: 2000, *Astron. Astrophys.* **363**, 269.
De Moortel, I., Hood, A. W., and Ireland, J.: 2002, *Astron. Astrophys.* **381**, 311.
De Pontieu, B., Martens, P. C. H., and Hudson, H. S.: 2001, *Astrophys. J.* **558**, 859.
Edwin, P. M. and Roberts, B.: 1983, *Solar Phys.* **88**, 179.
Goossens, M., Andries, J., and Aschwanden, M. J.: 2002, *Astron. Astrophys.* **394**, L39.
Handy, B. N., Acton, L. W., Kankelborg, C. C., Wolfson, C. J., Akin, D. J., Bruner, M. E., Caravalho, R., Catura, R. C., Chevalier, R., Duncan, D. W., Edwards, C. G., Feinstein, C. N., Freeland, S. L., Friedlaender, F. M., Hoffmann, C. H., Hurlburt, N. E., Jurcevich, B. K., Katz, N. L., Kelly, G. A., Lemen, J. R., Levay, M., Lindgren, R. W., Mathur, D. P., Meyer, S. B., Morrison, S. J., Morrison, M. D., Nightingale, R. W., Pope, T. P., Rehse, R. A., Schrijver, C. J., Shine, R. A., Shing, L., Strong, K. T., Tarbell, T. D., Title, A. M., Torgerson, D. D., Golub, L., Bookbinder, J. A., Caldwell, D., Cheimets, P. N., Davis, W. N., Deluca, E. E., McMullen, R. A., Warren, H. P., Amato, D., Fisher, R., Maldonado, H., and Parkinson, C.: 1999, *Solar Phys.* **187**, 229.
Kliem, B., Dammasch, I. E., Curdt, W., and Wilhelm, K.: 2002, *Astrophys. J. Lett.* **568**, L61.
Nakariakov, V. M. and Ofman, L.: 2001, *Astron. Astrophys.* **372**, 53.
Nakariakov, V. M., Ofman, L., DeLuca, E. E., Roberts, B., and Davila, J. M.: 1999, *Science* **285**, 862.
Ofman, L.: 2002, *Astrophys. J. Lett.* **568**, 135.
Ofman, L. and Aschwanden, M. J.: 2002, *Astrophys. J.* **576**, 153.
Oliver, R., Murawski, K., and Ballester, J. L.: 1998, *Astron. Astrophys.* **330**, 726.
Reeves, K. K., Shoer, J., Deluca, E. E., Winebarger, A. R., Ofman, L., and Davila, J. M.: 2001, *American Geophysical Union, Fall Meeting 2001, abstract #SH11A-0704*, A704.
Roberts, B., Edwin, P. M., and Benz, A. O.: 1984, *Solar Phys.* **279**, 857.
Roberts, B.: 2000, *Solar Phys.* **193**, 139.
Ruderman, M. S. and Roberts, B.: 2002, *Astrophys. J.* **577**, 475.
Schrijver, C. J. and Brown, D. S.: 2000, *Astrophys. J.* **537**, L69.
Schrijver, C. J., Aschwanden, M. J., and Title, A. M.: 2002, *Solar Phys.* **206**, 69.
Terradas, J., Oliver, R., and Ballester, J. L.: 1999, *Astrophys. J.* **517**, 488.
Thompson, B. J., Plunkett, S. P., Gurman, J. B., Newmark, J. S., St.Cyr, O. C., and Michels, D. J.: 1998, *Geophys. Res. Lett.* **25**, 2465.
Torrence, C. and Compo, G. P.: 1998, *Bull. Amer. Meteor. Soc.* **79**, 61.
Uchida, Y.: 1970, *Publ. Astron. Soc. Japan* **22**, 341.